arXiv:2610.38741v1 [cond-mat.str-el] 28 Oct 2026

Mixed-State Topological Transition and Emergent Fractionalized Supersymmetry in the Non-Abelian Kitaev Spin Liquid

Zhou-Quan Wan,[1] Hong Yao,[2,*] and Shao-Kai Jian[3,†]

[1]*Center for Computational Quantum Physics, Flatiron Institute, New York, New York 10010, USA*
[2]*Chen-Ning Yang Institute for Advanced Study (YIAS), Tsinghua University, Beijing 100084, China*
[3]*Department of Physics and Engineering Physics, Tulane University, New Orleans, Louisiana 70118, USA*

(Dated: October 30, 2026)

We study a mixed-state topological transition in the non-Abelian Kitaev spin liquid driven by a bond-dephasing channel. In the vectorized picture, bond dephasing maps onto interactions between two time-reversed fractionalized Majorana systems coupled to gapped $\mathbb{Z}_2$ gauge fields, enabling sign-problem-free Monte Carlo simulations. We show that increasing dephasing condenses an inter-copy fermion pair, converting $\mathrm{Ising} \boxtimes \overline{\mathrm{Ising}}$ to toric-code order in the Choi state and yielding intrinsically mixed-state topological order upon unfolding. More interestingly, at a temporal interface between topological and trivial Kitaev states, a Chern-number mismatch enforces a gapless Majorana mode. Dephasing then drives a mixed-state topological transition at which the gapless mode develops emergent $\mathcal{N}=1$ supersymmetry. Our Monte Carlo simulations yield $\nu = 1.27(3)$ and $\eta_b \simeq \eta_f \simeq 0.40$, consistent with the exact supersymmetric values $5/4$ and $2/5$. The supersymmetric partners are fractionalized and appear physically as distinct gauge-invariant spin strings, providing concrete observables for future experiments.

Introduction.—The organizing principles of quantum matter must be enlarged when a system is described by a mixed state rather than a ground-state wave function. Local dissipative evolution, monitoring, and decoherence motivate notions of phase equivalence that retain information inaccessible to observables linear in the density matrix [1–6]. A particularly sharp example is strong-to-weak spontaneous symmetry breaking (SW-SSB), in which independent left and right symmetry actions of the vectorized density matrix are reduced to their diagonal action [7–11]. The resulting order is detected by nonlinear Rényi correlators and has now become experimentally accessible in quantum platforms [12–15].

Decoherence also reorganizes topological order. Weak noise may leave encoded information recoverable, while stronger noise can drive sharp transitions in coherent information or Rényi correlations [16–23]. The Choi–Jamiołkowski map turns this problem into one of ordering in a doubled Hilbert space, where an error channel couples a topological theory to its time-reversed partner [24, 25]. Anyon condensation in the doubled state can then unfold to "gauging out" an anyon of the original density matrix, producing intrinsically mixed-state topological order (imTO) described by nonmodular anyon data and anomalous higher-form symmetry [26–31]. Nevertheless, what universal critical behavior can accompany a transition into such an intrinsically mixed phase remains largely open.

The chiral Kitaev honeycomb spin liquid is a particularly controlled setting for this question. Its spins fractionalize into itinerant Majorana fermions and static $\mathbb{Z}_2$ gauge fields, realizing Ising topological order in its non-Abelian phase [32, 33]. The Kitaev model and its associated spin-liquid phases have motivated extensive efforts toward realization in candidate materials and programmable quantum platforms [34–38]. The interplay of topology, fractionalization, and decoherence provides a natural setting for unconventional critical phenomena. In particular, interacting fermionic and bosonic degrees of freedom can give rise to emergent spacetime supersymmetry [39–48]. Whether such physics can arise at a decoherence-driven transition involving intrinsically mixed-state topological order remains unexplored.

In this Letter, we uncover unconventional mixed-state criticality in the dephased Kitaev spin liquid. We first show that bond dephasing drives inter-copy fermion condensation, converting $\mathrm{Ising} \boxtimes \overline{\mathrm{Ising}}$ into toric-code order in the Choi state; upon unfolding, the maximal-dephasing fixed point realizes imTO with a transparent fermion. We then study a temporal interface between topological and trivial Kitaev states, where the Chern-number mismatch enforces a gapless Majorana mode. Dephasing tunes this topology-constrained critical phase to a tricritical-Ising endpoint with emergent $\mathcal{N}=1$ spacetime supersymmetry. Our sign-problem-free quantum Monte Carlo simulations yield critical exponents and matching bosonic and fermionic anisotropies, consistent with the supersymmetric predictions. We also discuss the supersymmetric partners that are encoded in distinct gauge-invariant spin strings rather than local microscopic operators.

Model and doubled Hilbert space.—We consider the spin-$1/2$ Kitaev honeycomb model with a time-reversal-breaking three-spin interaction, as shown in Fig. 1(a),

$$H = -\sum_{\langle ij\rangle_\alpha} J_\alpha \sigma_i^\alpha \sigma_j^\alpha - \kappa \sum_{\langle\langle ik\rangle\rangle} \sigma_i^\alpha \sigma_j^\gamma \sigma_k^\beta. \tag{1}$$

Here J_α is the exchange coupling on a nearest-neighbor bond $\langle ij\rangle_\alpha$ of type $\alpha = x, y, z$, and $B_{ij}^\alpha \equiv \sigma_i^\alpha \sigma_j^\alpha$ is the corresponding bond operator. The second sum runs over oriented next-nearest-neighbor pairs $\langle\langle ik\rangle\rangle$, with j the intermediate site along $i \xrightarrow{\alpha} j \xrightarrow{\beta} k$ and γ the remaining spin component. The κ term breaks time-reversal symmetry and can gap the Majorana cones, yielding non-Abelian Ising topological order [32].

Starting from a ground-state projector ρ_0 in this phase, we apply dephasing on each bond [49]:

$$\mathcal{E}_{ij}^\alpha(\rho) = (1-p)\rho + pB_{ij}^\alpha \rho B_{ij}^\alpha, \qquad 0 \le p \le \tfrac{1}{2}, \tag{2}$$

and the full channel $\mathcal{E}_p$ is the product over all bonds; we write $\rho_p = \mathcal{E}_p(\rho_0)$. This dephasing channel preserves all plaquette

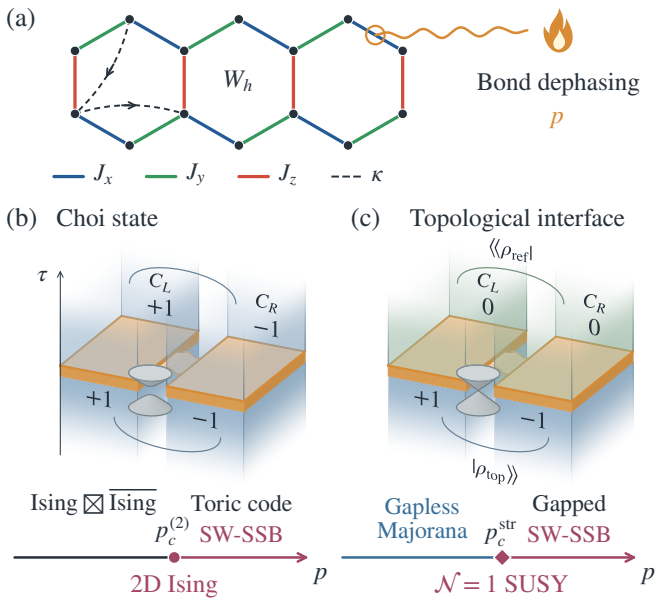


FIG. 1. (a) Kitaev honeycomb model with bond couplings J_x, J_y, J_z and chiral coupling κ. Dashed arrows indicate oriented next-nearest-neighbor hopping, and W_h denotes the plaquette flux. Bond dephasing acts as $\mathcal{E}_{ij}^{\alpha}(\rho) = (1-p)\rho + pB_{ij}^{\alpha}\rho B_{ij}^{\alpha}$. (b) Choi-state geometry with no Chern mismatch across the temporal interface. Increasing p condenses the inter-copy boson $\psi\bar{\psi}$, producing SW-SSB and converting Ising $\boxtimes$ $\overline{\text{Ising}}$ topological order into toric-code order. The transition at $p_c^{(2)}$ belongs to the two-dimensional Ising universality class. (c) Temporal interface between topological and trivial states. The Chern mismatch $|\Delta C| = 1$ supports a gapless Majorana mode at weak dephasing. Increasing p drives a transition into a gapped phase through the fractionalized $\mathcal{N} = 1$ supersymmetric critical point at $p_c^{\rm str}$.

fluxes $W_h = \prod_{n=1}^{6}\sigma_n^{\beta_n}$, where the sites are ordered around hexagon h and β_n labels the bond leaving the hexagon at site n. The initial ground state lies in the zero-flux sector, with $W_h = +1$ on every hexagon. Since $[B_{ij}^{\alpha}, W_h] = 0$ for every bond and plaquette, ρ_p remains in this sector.

To study the mixed-state ordering induced by dephasing, we vectorize the density matrix as $|\rho\rangle\rangle = (\rho\otimes\mathbb{1})|\Omega\rangle\rangle$, where $|\Omega\rangle\rangle = \prod_i(|\uparrow\uparrow\rangle_i + |\downarrow\downarrow\rangle_i)/\sqrt{2}$ and $O_L|\Omega\rangle\rangle = O_R^T|\Omega\rangle\rangle$ [24, 25]. The doubled Hilbert space consists of a left copy (L) and a right copy (R), representing the ket and bra indices of ρ, respectively. Writing $D_{ij}^{\alpha} = B_{ij,L}^{\alpha}B_{ij,R}^{\alpha}$, the channel in Eq. (2) becomes

$$\widehat{\mathcal{E}}(p) = \prod_{\alpha,\langle ij\rangle_\alpha}[(1-p)\mathbb{1} + pD_{ij}^{\alpha}] \propto e^{V(p)\sum_{\alpha,\langle ij\rangle_\alpha} D_{ij}^{\alpha}}, \quad (3)$$

where $V(p) = -\frac{1}{2}\ln(1-2p)$. This exponential representation is exact up to an overall scalar: $(D_{ij}^{\alpha})^2 = 1$, and all such operators commute because anticommutation signs cancel between the two copies. Thus dephasing generates an inter-copy coupling whose strength increases with p.

Fractionalization.—We fractionalize each spin as $\sigma_{i,s}^{\alpha} = \mathrm{i}b_{i,s}^{\alpha}c_{i,s}$, subject to the local constraint $G_{i,s} = b_{i,s}^{x}b_{i,s}^{y}b_{i,s}^{z}c_{i,s} = 1$, where $s = L, R$. Following the convention detailed in the Supplemental Material [50], we define $u_{ij,s} = \mathrm{i}\zeta_s b_{i,s}^{\alpha}b_{j,s}^{\alpha}$, with $\zeta_L = -\zeta_R = 1$ and $u_{ji,s} = -u_{ij,s}$. The physical state is obtained by gauge projection, while $W_{h,s} = \prod_{\langle ij\rangle\in\partial h} u_{ij,s}$ is gauge invariant; the plaquette product uses the fixed A-to-B orientation on every bond. The bond-dephasing channel commutes with all static link operators $u_{ij,s}$ and hence preserves each flux sector. We work in a fixed zero-flux sector with $u_{ij,L} = u_{ij,R}$; the boundary conditions and physical projection are specified in the Supplemental Material [50]. The matter Hamiltonians then read

$$H_s = \zeta_s\left(\mathrm{i}\sum_{\alpha,\langle ij\rangle_\alpha} J_\alpha c_{i,s}c_{j,s} + \mathrm{i}\kappa\sum_{\langle\langle ik\rangle\rangle}\nu_{ik}c_{i,s}c_{k,s}\right). \quad (4)$$

Here $\nu_{ik} = \epsilon_{\alpha\beta\gamma} = -\nu_{ki}$, with $\epsilon_{xyz} = 1$, for the oriented path defined above. The two Hamiltonians satisfy $H_R = H_L^*$ and therefore have opposite matter-band Chern numbers.

In this gauge convention, the bond-dephasing channel in Eq. (3) becomes $\widehat{\mathcal{E}}(p) \propto \exp[V(p)\sum_{\langle ij\rangle}\Phi_i\Phi_j]$, corresponding to a ferromagnetic coupling of the inter-copy Majorana bilinear $\Phi_i = \mathrm{i}c_{i,L}c_{i,R}$. This provides the tunable inter-copy interaction that will later control the temporal-interface criticality. An exact Hubbard–Stratonovich decomposition and Majorana positivity make this interacting problem accessible to sign-problem-free Monte Carlo simulations; the construction and estimators are given in the Supplemental Material [50–54].

Topological transition.—We first consider the normalized Choi state, whose overlap geometry is illustrated in Fig. 1(b). The coupling $V(p)\sum_{\langle ij\rangle}\Phi_i\Phi_j$ grows monotonically with dephasing and eventually drives an inter-copy pairing instability. However, Φ_i is gauge charged: under the independent $\mathbb{Z}_2$ gauge transformations of the two copies, $c_{i,s} \to \lambda_{i,s}c_{i,s}$ and $u_{ij,s} \to \lambda_{i,s}u_{ij,s}\lambda_{j,s}$, it transforms as $\Phi_i \to \lambda_{i,L}\lambda_{i,R}\Phi_i$. A physical pairing correlator must therefore connect its endpoints by a $\mathbb{Z}_2$ gauge string in each copy.

For an oriented path $\gamma : i \to j$, define the Wilson string $U_{\gamma,s} = \prod_{\langle lm\rangle\in\gamma} u_{lm,s}$. The gauge-invariant Rényi-2 pairing correlator of the Choi state $|\rho_p\rangle\rangle = \widehat{\mathcal{E}}(p)|\rho_0\rangle\rangle$ is

$$\mathcal{C}_{\Phi}^{(2)}(i,j;\gamma) = \frac{\langle\langle\rho_p|\Phi_i U_{\gamma,L}U_{\gamma,R}\Phi_j|\rho_p\rangle\rangle}{\langle\langle\rho_p|\rho_p\rangle\rangle}. \quad (5)$$

The Wilson strings cancel the endpoint gauge charges. Since the two copies have identical link configurations, $U_{\gamma,L}U_{\gamma,R} = 1$, so this expression reduces to the normalized Choi correlator of $\Phi_i\Phi_j$. It is unchanged under contractible path deformations within the zero-flux sector.

For $J_x = J_y = J_z = 1$ and $\kappa = 1/2$, we take $|\rho_0\rangle\rangle$ from the non-Abelian Ising topological phase. Fig. 2(a) shows a clear common crossing of the dimensionless correlation ratio $R_{\Phi}^{(2)}$. Its finite-size flow reverses across the crossing, decreasing with L on the weak-dephasing side and increasing on the strong-dephasing side, signaling a transition from the disordered phase to an inter-copy condensed phase. A finite-size collapse of $R_{\Phi}^{(2)}$ and the pairing order parameter m_{Φ}^2 in Fig. 2(b) yields $p_c^{(2)} =$

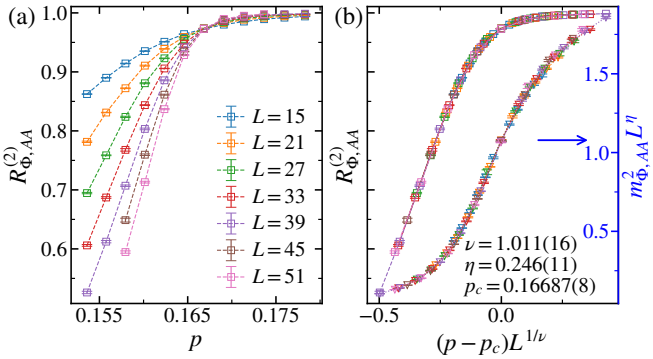


FIG. 2. Inter-copy condensation in the normalized Choi state. (a) Rényi-2 Wilson-string correlation ratio $R^{(2)}_\Phi = 1 - S^{(2)}_\Phi(\boldsymbol{q}_{\min})/S^{(2)}_\Phi(\boldsymbol{0})$ for $L = 15, 21, \ldots, 51$. Here $S^{(2)}_\Phi(\boldsymbol{q}) = L^{-2}\sum_{i,j\in A} e^{\mathrm{i}\boldsymbol{q}\cdot(\boldsymbol{r}_i-\boldsymbol{r}_j)}\mathcal{C}^{(2)}_\Phi(i,j;\gamma_{ij})$ and $\boldsymbol{q}_{\min}$ is the smallest nonzero momentum. (b) Finite-size collapses of the correlation ratio (left axis) and $m^2_\Phi L^\eta$ (right axis), with $m^2_\Phi = S^{(2)}_\Phi(\boldsymbol{0})/L^2$, versus $(p-p_c^{(2)})L^{1/\nu}$. The fits yield $p_c^{(2)} = 0.16687(8)$, $\nu = 1.011(16)$, and $\eta = 0.246(11)$, consistent with the two-dimensional Ising values $\nu = 1$ and $\eta = 1/4$. See Supplemental Material [50] for details.

$0.16687(8)$, $\nu = 1.011(16)$, and $\eta = 0.246(11)$, consistent with the two-dimensional Ising transition, $\nu = 1$ and $\eta = 1/4$.

The ordered phase identified above has a direct symmetry interpretation. Since Φ is odd under either copy fermion parity but even under their product, its long-range order realizes the fermion-parity SW-SSB pattern $\mathbb{Z}^f_{2,L} \times \mathbb{Z}^f_{2,R} \to \mathbb{Z}^f_{2,\mathrm{diag}}$. From the anyon perspective, after gauge projection a matter-Majorana endpoint corresponds to the Ising fermion anyon ψ and must be attached to a $\mathbb{Z}_2$ Wilson line. The gauge-invariant string operator in Eq. (5) therefore creates a $\psi\bar{\psi}$ boson at each endpoint. Thus the transition is an anyon $\psi\bar{\psi}$ condensation transition in the normalized Choi state [30], as shown in Fig. 1(b).

Viewed as a pure state in the doubled Hilbert space, $|\rho_0\rangle\!\rangle$ has Ising $\boxtimes$ $\overline{\text{Ising}}$ topological order, with sectors $a\bar{b}$ for $a, b \in \{1, \sigma, \psi\}$. Condensation of $\psi\bar{\psi}$ identifies sectors related by fusion with the condensate and confines those with nontrivial monodromy. Thus $1\bar{1} \sim \psi\bar{\psi}$ and $\psi\bar{1} \sim 1\bar{\psi} \equiv \epsilon$. The sector $\sigma\bar{\sigma}$ is invariant under fusion with $\psi\bar{\psi}$ and, having quantum dimension two, splits as $e + m$. Consequently [55–58],

$$\text{Ising} \boxtimes \overline{\text{Ising}} \xrightarrow{\psi\bar{\psi}} \{1, e, m, \epsilon\}_{\mathrm{TC}},$$

yielding the toric-code topological order.

Unfolding changes the interpretation of this condensation. The right copy is the bra index, and $\psi\bar{\psi}$ represents the quantum channel $\rho \mapsto W_\psi \rho W_\psi^\dagger$ rather than an independent bilayer anyon. The transition therefore gauges out ψ instead of simply declaring it the vacuum [28]. This gauging-out process has a higher-form SW-SSB manifestation. Because a one-sided σ Wilson loop has monodromy -1 with $\psi\bar{\psi}$, its independent left and right actions cease to be strong symmetries, while their diagonal action survives as a weak symmetry. By contrast, the ψ Wilson loop has trivial monodromy with the condensate and remains a strong symmetry. The surviving strong sector is therefore $\{1, \psi\}$, in which ψ is a transparent fermion, rendering the sector nonmodular. Assuming no intervening transition, the ordered branch is continuously connected to the maximal-dephasing endpoint, which is an imTO fixed point [27–29].

Emergent supersymmetry.—Having established the bulk dephasing transition and its mixed-state topological interpretation, we now ask how the same dephasing acts on an interface enforced by a change of topology. We construct the temporal interface shown in Fig. 1(c) by pairing the non-Abelian Kitaev state with an Abelian reference state whose matter band is topologically trivial. This interface is naturally probed by the mixed-state strange correlator [59–63],

$$\langle\mathcal{O}\rangle_{\mathrm{str}} = \frac{\langle\!\langle\rho_{\mathrm{ref}}|\mathcal{O}\widehat{\mathcal{E}}(p)|\rho_{\mathrm{top}}\rangle\!\rangle}{\langle\!\langle\rho_{\mathrm{ref}}|\widehat{\mathcal{E}}(p)|\rho_{\mathrm{top}}\rangle\!\rangle}. \tag{6}$$

Here $|\rho_{\mathrm{top}}\rangle\!\rangle$ and $|\rho_{\mathrm{ref}}\rangle\!\rangle$ are the vectorized ground-state projectors of Eq. (1) with $J_x = J_y = J > 0$, $\kappa > 0$, $0 < J_z^{\mathrm{top}} < 2J$, and $J_z^{\mathrm{ref}} > 2J$, respectively. Unlike the normalized Choi correlator in Eq. (5), the strange overlap involves a single factor of $\widehat{\mathcal{E}}(p)$ and different boundary states. Its critical probability, denoted by p_c, need not coincide with $p_c^{(2)}$. The Chern-number mismatch produces one chiral Majorana mode in each copy [64], forming a nonchiral Majorana field whose bilinear mass is forbidden by the independent copy parities; the temporal interface is therefore gapless at weak dephasing. To obtain its propagator, combine the two sublattice matter Majoranas, after a fixed basis rotation, into $f_{\boldsymbol{q},s} = (c_{A,\boldsymbol{q},s} + \mathrm{i}\zeta_s c_{B,\boldsymbol{q},s})/2$. Near the band inversion, the topological state has a singular BCS pair amplitude, while the trivial reference state can be flattened to the empty f vacuum without affecting this singularity. Time reversal relates the two copies, so at $p = 0$,

$$\langle f_{L,\boldsymbol{q}} f_{L,-\boldsymbol{q}}\rangle_{\mathrm{str}} = -\langle f_{R,\boldsymbol{q}} f_{R,-\boldsymbol{q}}\rangle^*_{\mathrm{str}} \sim \frac{1}{v_{fx}q_x + \mathrm{i}v_{fy}q_y}. \tag{7}$$

The detailed BCS-overlap derivation is given in the Supplemental Material [50]. The inverse of the singular propagators in Eq. (7) fixes the universal quadratic action,

$$S_M[\chi] = \frac{1}{2}\int \frac{d^2q}{(2\pi)^2}\, \chi^T_{-\boldsymbol{q}}(\mathrm{i}v_{fy}q_y\mathbb{1} + v_{fx}q_x\sigma^z)\chi_{\boldsymbol{q}}, \tag{8}$$

where χ denotes the long-wavelength chiral Majorana field associated with the singular part of the microscopic f field and σ^z acts in the (χ_L, χ_R) copy/chirality space. The two components are exchanged by the time-reversal-like copy operation and together form a nonchiral Ising Majorana field theory with central charge $c = 1/2$.

The gauge sector contributes no additional critical mode: plaquette fluxes are conserved, so the dynamics remains exactly within the zero-flux sector. More generally, gapped vison excitations only renormalize local couplings and do not introduce additional relevant perturbation [32, 48]. The relevant degrees of freedom at the criticality are therefore the inter-copy scalar ϕ—the continuum counterpart of the gauge-invariant completion of Φ—and the gapless Majorana mode χ.

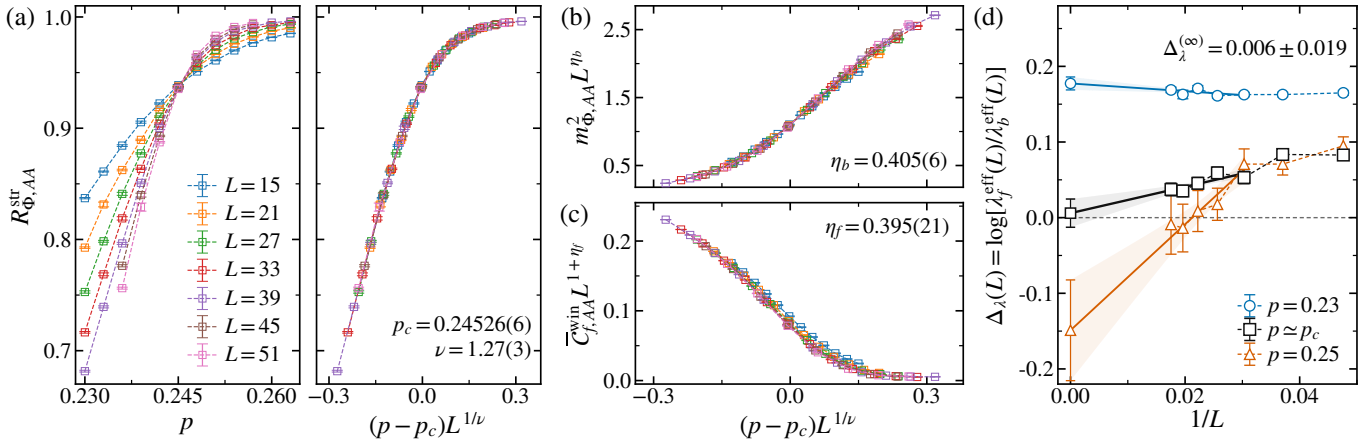


FIG. 3. Emergent supersymmetry at the temporal interface. (a) Inter-copy correlation ratio $R^{\mathrm{str}}_{\Phi,AA}$ for $L=15,21,\ldots,51$ (left) and its finite-size collapse (right), yielding $p_c=0.24526(6)$ and $\nu=1.27(3)$. (b),(c) Data collapses of the rescaled bosonic estimator $m^2_{\Phi,AA}L^{\eta_b}$ and window-averaged fermionic string correlator $\overline{\mathcal{C}}^{\mathrm{win}}_{f,AA}L^{1+\eta_f}$, respectively. Independent fits give $\eta_b=0.405(6)$ and $\eta_f=0.395(21)$, consistent with the supersymmetry predictions $\eta_b=\eta_f=2/5$ and $\nu_p=5/4$. The fits in (b),(c) use p_c and ν from (a), with their uncertainties propagated through bootstrap resampling. (d) Finite-size anisotropy mismatch $\Delta_\lambda(L)=\ln[\lambda_f^{\mathrm{eff}}(L)/\lambda_b^{\mathrm{eff}}(L)]$ versus $1/L$, with λ_b^{eff} and λ_f^{eff} extracted from directional AA correlation ratios. Solid lines show linear fits in $1/L$, and symbols at $1/L=0$ denote the extrapolated intercepts. The near-critical data yield an intercept of $0.006(19)$, consistent with zero mismatch, marked by the horizontal dashed line. Details of the simulation setup and finite-size scaling analysis are provided in the Supplemental Material [50].

Including the scalar kinetic, mass, and quartic terms gives the Majorana–Ising Yukawa action

$$S = S_M[\chi] + \int d^2x \left(\tfrac{1}{2}[(v_{bx}\partial_x\phi)^2+(v_{by}\partial_y\phi)^2] + \tfrac{r}{2}\phi^2 + \tfrac{u}{4!}\phi^4 + g\phi\, \mathrm{i}\chi_R\chi_L\right), \tag{9}$$

where r and u are the quadratic and quartic scalar couplings, and g is the Yukawa coupling.

Since dephasing preserves the copy parities, varying p tunes interactions along the gapless Ising manifold until ϕ becomes critical. Importantly, emergent supersymmetry does not require microscopic spatial isotropy. It has been shown that the relative boson–fermion anisotropy, λ_f/λ_b, with $\lambda_a=v_{ay}/v_{ax}$ for $a=b,f$, flows to one, $(\lambda_f/\lambda_b)_*=1$, at the infrared fixed point [41, 43, 48]. Thus the bosonic and fermionic metrics flow to a common form, which may be chosen isotropic by coordinate rescaling. After this rescaling, the renormalized couplings approach the supersymmetric manifold $r_*=0$ and $u_*=3g_*^2$. The resulting fixed point is the tricritical-Ising CFT, with $c=7/10$ and emergent $\mathcal{N}=1$ spacetime supersymmetry [39, 65–67]. At the fixed point, the bosonic field ϕ overlaps with ϵ, with scaling dimension $x_\epsilon=1/5$, while the Majorana field χ overlaps with its fermionic superpartner ψ_ϵ, with $x_{\psi_\epsilon}=7/10$ [68]. Their correlations therefore decay as $\langle\phi(\boldsymbol{r})\phi(\boldsymbol{0})\rangle_{\mathrm{str}}\sim r^{-\eta_b}$ and $\langle\chi(\boldsymbol{r})\chi(\boldsymbol{0})\rangle_{\mathrm{str}}\sim r^{-(1+\eta_f)}$. Supersymmetry requires $\eta_b=\eta_f$, with the common value $2/5$ at the tricritical-Ising fixed point.

We test these predictions using gauge-invariant lattice string correlators. The bosonic correlator uses the Wilson-line completion introduced above, now evaluated with $\mathcal{C}_b(i,j;\gamma)=\langle\Phi_iU_{\gamma,L}U_{\gamma,R}\Phi_j\rangle_{\mathrm{str}}$. Its fermionic counterpart is $\mathcal{C}_f(i,j;\gamma)=\mathrm{i}\,\langle c_{i,L}U_{\gamma,L}c_{j,L}\rangle_{\mathrm{str}}$. The bosonic and fermionic strings are type-II and type-I strange correlators, respectively [21]. They provide gauge-invariant probes of the fractionalized supermultiplet [48].

For finite-size analysis, we use the bosonic diagnostics R^{str}_Φ and m^2_Φ, defined analogously to those in the Choi-state analysis, together with the window-averaged fermionic correlator

$$\overline{\mathcal{C}}^{\mathrm{win}}_f = \frac{1}{|\mathcal{W}_L|}\sum_{\boldsymbol{d}\in\mathcal{W}_L}|\mathcal{C}_{f,AA}(\boldsymbol{d})|\,. \tag{10}$$

All estimators use translation-averaged AA correlations, and $|\mathcal{W}_L|$ counts the displacements in the averaging window. At criticality, $m^2_\Phi\sim L^{-\eta_b}$ and $\overline{\mathcal{C}}^{\mathrm{win}}_f\sim L^{-1-\eta_f}$. The spin-string representations, lattice and window conventions, and numerical procedures are detailed in the Supplemental Material [50]. Fig. 3(a) shows a common crossing of R^{str}_Φ for $L=15,21,\ldots,51$. Its finite-size collapse gives $p_c=0.24526(6)$ and $\nu=1.27(3)$, consistent with the predicted $\nu_p=5/4$ [69]. Holding p_c and ν fixed, independent fits of the bosonic and fermionic observables in Fig. 3(b)(c) yield $\eta_b=0.405(6)$ and $\eta_f=0.395(21)$, consistent with the emergent supersymmetry.

Beyond the scaling exponents, we compare the spatial anisotropies of the two sectors using their AA correlators at $\boldsymbol{d}_\pm=\frac{L}{3}(\boldsymbol{a}_1\pm\boldsymbol{a}_2)$. These displacements lie along the Cartesian axes and satisfy $|\boldsymbol{d}_-|/|\boldsymbol{d}_+|=\sqrt{3}$. Motivated by the anisotropic critical power laws, we define the finite-size estimators

$$\lambda_a^{\mathrm{eff}}(L)=\sqrt{3}\left|\frac{\mathcal{C}_{a,AA}(\boldsymbol{d}_-)}{\mathcal{C}_{a,AA}(\boldsymbol{d}_+)}\right|^{1/\alpha_a}, \qquad a=b,f, \tag{11}$$

where we fix $\alpha_b=2/5$ and $\alpha_f=7/5$ to the supersymmetric

predictions. Fig. 3(d) shows the relative anisotropy $\Delta_\lambda(L) = \log[\lambda_f^{\rm eff}(L)/\lambda_b^{\rm eff}(L)]$, together with fits to $\Delta_\lambda(L) = \Delta_\lambda^{(\infty)} + A_\lambda/L$. At $p \simeq p_c$, the extrapolated mismatch is compatible with zero, providing a complementary consistency check of matching bosonic and fermionic correlation anisotropies.

Concluding remarks.—We have identified two complementary universal structures generated by bond dephasing of a non-Abelian Kitaev spin liquid. In the two-dimensional Choi construction, a Rényi-2 Wilson-string correlator locates an inter-copy anyon condensation transition from doubled-Ising to toric-code order; unfolding this condensate at the maximal-dephasing fixed point gives imTO with a transparent fermion. More interestingly, at a temporal interface with a trivial reference state, the Chern mismatch supplies gapless Majorana modes. The resulting transition is instead the tricritical-Ising fixed point with emergent fractionalized $\mathcal{N} = 1$ supersymmetry.

Our predictions are in principle accessible on programmable spin platforms that can prepare topological states and probe anyonic observables [70–72]. The gauge-invariant bosonic and fermionic strings can be accessed through a spin-based two-copy measurement protocol involving local Bell readout, with the prescribed dephasing incorporated in classical postprocessing. Beyond the integrable limit, we expect this criticality to persist while the vison gap remains open and gauge fluctuations generate no additional relevant perturbation.

Acknowledgments: This work is supported in part by the NSFC under Grant Nos. 12347107 and 12334003 (H.Y.) and by the New Cornerstone Science Foundation through the Xplorer Prize (H.Y.). The Flatiron Institute is a division of the Simons Foundation. We used the AI tool GPT models (GPT-5.6 and GPT-6) to assist with manuscript editing.

* yaohong@tsinghua.edu.cn
† sjian@tulane.edu

[1] A. Coser and D. Pérez-García, Classification of phases for mixed states via fast dissipative evolution, Quantum **3**, 174 (2019).
[2] C. de Groot, A. Turzillo, and N. Schuch, Symmetry protected topological order in open quantum systems, Quantum **6**, 856 (2022).
[3] M. McGinley and N. R. Cooper, Classification of topological insulators and superconductors out of equilibrium, Phys. Rev. B **99**, 075148 (2019).
[4] A. Altland, M. Fleischhauer, and S. Diehl, Symmetry classes of open fermionic quantum matter, Phys. Rev. X **11**, 021037 (2021).
[5] Z. Liu, L. Chen, Y. Zhang, S. Zhou, and P. Zhang, Diagnosing strong-to-weak symmetry breaking via Wightman correlators, Communications Physics **8**, 274 (2025).
[6] T.-H. Yang, B. Shi, and J. Y. Lee, Topological mixed states: Phases of matter from axiomatic approaches, Physical Review X **16**, 041002 (2026).
[7] J. Y. Lee, C.-M. Jian, and C. Xu, Quantum criticality under decoherence or weak measurement, PRX Quantum **4**, 030317 (2023).
[8] L. A. Lessa, R. Ma, J.-H. Zhang, Z. Bi, M. Cheng, and C. Wang, Strong-to-weak spontaneous symmetry breaking in mixed quantum states, PRX Quantum **6**, 010344 (2025).
[9] P. Sala, S. Gopalakrishnan, M. Oshikawa, and Y. You, Spontaneous strong symmetry breaking in open systems: Purification perspective, Phys. Rev. B **110**, 155150 (2024).
[10] Z. Weinstein, Efficient detection of strong-to-weak spontaneous symmetry breaking via the Rényi-1 correlator, Phys. Rev. Lett. **134**, 150405 (2025).
[11] D. Gu, Z. Wang, and Z. Wang, Spontaneous symmetry breaking in open quantum systems: Strong, weak, and strong-to-weak, Phys. Rev. B **112**, 245123 (2025).
[12] S. Wang, T. G. Kiely, D. Tell, J. Obermeyer, M. Barendregt, P. Bojović, P. M. Preiss, A. Sarma, T. Franz, M. P. A. Fisher, C. Xu, and I. Bloch, Observation of strong-to-weak spontaneous symmetry breaking in a dephased Fermi gas (2026), arXiv:2604.16137 [cond-mat.quant-gas].
[13] Q. Cao, Z. Bi, and K. W. Murch, Mixed-state symmetry-protected topology and strong-to-weak spontaneous symmetry breaking in a superconducting qubit array, arXiv preprint arXiv:2608.24993 (2026).
[14] Z.-Y. Wei, C. Fechisin, Y.-X. Wang, J. Shah, T.-C. Lu, C.-J. Lin, and A. V. Gorshkov, Strong-to-weak spontaneous symmetry breaking transitions on a quantum processor (2026), arXiv:2610.26229 [quant-ph].
[15] Y. Zhang, T. H. Hsieh, Y. B. Kim, and Y. Zou, Probing mixed-state phases on a quantum computer via Renyi correlators and variational decoding, Nature Communications **17**, 8047 (2026).
[16] E. Dennis, A. Kitaev, A. Landahl, and J. Preskill, Topological quantum memory, J. Math. Phys. **43**, 4452 (2002).
[17] Y. Bao, R. Fan, A. Vishwanath, and E. Altman, Mixed-state topological order and the errorfield double formulation of decoherence-induced transitions, Phys. Rev. Lett. **136**, 220402 (2026).
[18] R. Fan, Y. Bao, E. Altman, and A. Vishwanath, Diagnostics of mixed-state topological order and breakdown of quantum memory, PRX Quantum **5**, 020343 (2024).
[19] S. Sang, Y. Zou, and T. H. Hsieh, Mixed-state quantum phases: Renormalization and quantum error correction, Phys. Rev. X **14**, 031044 (2024).
[20] Y.-H. Chen and T. Grover, Symmetry-enforced many-body separability transitions, PRX Quantum **5**, 030310 (2024).
[21] J. Y. Lee, Y.-Z. You, and C. Xu, Symmetry protected topological phases under decoherence, Quantum **9**, 1607 (2025).
[22] P. Sala, J. Alicea, and R. Verresen, Decoherence and wavefunction deformation of D_4 non-abelian topological order, Physical Review X **15**, 031002 (2025).
[23] A. Vadali, R. Vanhove, R. Verresen, J. Alicea, and P. Sala, Statistical mechanics and symmetries of non-abelian anyon proliferation: From deformation to decoherence (2026), arXiv:2606.12527 [quant-ph].
[24] A. Jamiołkowski, Linear transformations which preserve trace and positive semidefiniteness of operators, Rep. Math. Phys. **3**, 275 (1972).
[25] M.-D. Choi, Completely positive linear maps on complex matrices, Linear Algebra Appl. **10**, 285 (1975).
[26] Z. Wang, Z. Wu, and Z. Wang, Intrinsic mixed-state topological order, PRX Quantum **6**, 010314 (2025).
[27] T. D. Ellison and M. Cheng, Toward a classification of mixed-state topological orders in two dimensions, PRX Quantum **6**, 010315 (2025).
[28] R. Sohal and A. Prem, Noisy approach to intrinsically mixed-state topological order, PRX Quantum **6**, 010313 (2025).
[29] C. Zhang, Y. Xu, J.-H. Zhang, C. Xu, Z. Bi, and Z.-X. Luo, Strong-to-weak spontaneous breaking of 1-form symmetry and intrinsically mixed topological order, Phys. Rev. B **111**, 115137 (2025).
[30] Z. Li and R. S. K. Mong, Replica topological order in quantum

mixed states and quantum error correction, Phys. Rev. B **111**, 125106 (2025).
[31] S. Zhang, L. Li, Z. Bi, T.-C. Wei, and Z. Song, Decohering kitaev's sixteenfold way: A holographic approach (2026), arXiv:2610.03610 [cond-mat.str-el].
[32] A. Kitaev, Anyons in an exactly solved model and beyond, Ann. Phys. **321**, 2 (2006).
[33] C. Nayak, S. H. Simon, A. Stern, M. Freedman, and S. Das Sarma, Non-Abelian anyons and topological quantum computation, Rev. Mod. Phys. **80**, 1083 (2008).
[34] G. Jackeli and G. Khaliullin, Mott insulators in the strong spin-orbit coupling limit: From Heisenberg to a quantum compass and Kitaev models, Phys. Rev. Lett. **102**, 017205 (2009).
[35] M. Hermanns, I. Kimchi, and J. Knolle, Physics of the Kitaev model: Fractionalization, dynamic correlations, and material connections, Annu. Rev. Condens. Matter Phys. **9**, 17 (2018).
[36] C. Broholm, R. J. Cava, S. A. Kivelson, D. G. Nocera, M. R. Norman, and T. Senthil, Quantum spin liquids, Science **367**, eaay0668 (2020).
[37] S. J. Evered, M. Kalinowski, A. A. Geim, T. Manovitz, D. Bluvstein, S. H. Li, N. Maskara, H. Zhou, S. Ebadi, M. Xu, *et al.*, Probing the kitaev honeycomb model on a neutral-atom quantum computer, Nature **645**, 341 (2025).
[38] A. Ali, J. Gibbs, K. Kumaran, V. Muruganandam, B. Xiao, P. Kairys, G. B. Halász, A. Banerjee, and P. C. Lotshaw, Probing chiral topological order of the Kitaev honeycomb on a trapped ion processor, PRX Quantum 10.1103/wj7x-kwdg (2026), accepted 20 October 2026, arXiv:2507.08939 [quant-ph].
[39] D. Friedan, Z. Qiu, and S. Shenker, Conformal invariance, unitarity, and critical exponents in two dimensions, Phys. Rev. Lett. **52**, 1575 (1984).
[40] S.-S. Lee, Emergence of supersymmetry at a critical point of a lattice model, Phys. Rev. B **76**, 075103 (2007).
[41] T. Grover, D. N. Sheng, and A. Vishwanath, Emergent space-time supersymmetry at the boundary of a topological phase, Science **344**, 280 (2014).
[42] P. Ponte and S.-S. Lee, Emergence of supersymmetry on the surface of three-dimensional topological insulators, New J. Phys. **16**, 013044 (2014).
[43] S.-K. Jian, Y.-F. Jiang, and H. Yao, Emergent spacetime supersymmetry in 3D Weyl semimetals and 2D Dirac semimetals, Phys. Rev. Lett. **114**, 237001 (2015).
[44] A. Rahmani, X. Zhu, M. Franz, and I. Affleck, Emergent supersymmetry from strongly interacting Majorana zero modes, Phys. Rev. Lett. **115**, 166401 (2015).
[45] S.-K. Jian, C.-H. Lin, J. Maciejko, and H. Yao, Emergence of supersymmetric quantum electrodynamics, Phys. Rev. Lett. **118**, 166802 (2017).
[46] Z.-X. Li, Y.-F. Jiang, and H. Yao, Edge quantum criticality and emergent supersymmetry in topological phases, Phys. Rev. Lett. **119**, 107202 (2017).
[47] Y. Ge, H. Jiang, H. Yao, and S.-K. Jian, Boundary criticality in two-dimensional correlated topological superconductors, arXiv preprint arXiv:2510.05230 (2025).
[48] Z. Wu, Z.-Q. Wan, S.-K. Jian, and H. Yao, Emergent spacetime supersymmetry at 2D fractionalized quantum criticality, Phys. Rev. Lett. **136**, 256502 (2026).
[49] K. Hwang, Mixed-state quantum spin liquids and dynamical anyon condensations in Kitaev lindbladians, Quantum **8**, 1412 (2024).
[50] See Supplemental Material for vectorization conventions, the exact dephasing decomposition, simulation estimators and scaling forms, anyon condensation, the interface-mode derivation, tricritical-Ising operator matching, and gauge-invariant string observables.
[51] Z.-X. Li, Y.-F. Jiang, and H. Yao, Solving the fermion sign problem in quantum Monte Carlo simulations by Majorana representation, Phys. Rev. B **91**, 241117(R) (2015).
[52] Z.-X. Li, Y.-F. Jiang, and H. Yao, Majorana-time-reversal symmetries: A fundamental principle for sign-problem-free quantum Monte Carlo simulations, Phys. Rev. Lett. **117**, 267002 (2016).
[53] Z. C. Wei, C. Wu, Y. Li, S. Zhang, and T. Xiang, Majorana positivity and the fermion sign problem of quantum Monte Carlo simulations, Phys. Rev. Lett. **116**, 250601 (2016).
[54] Y. Xue, Z. Cheng, and M. Ippoliti, Simulation of bilayer hamiltonians based on monitored quantum trajectories, Phys. Rev. B **113**, 094312 (2026).
[55] F. A. Bais and J. K. Slingerland, Condensate-induced transitions between topologically ordered phases, Phys. Rev. B **79**, 045316 (2009).
[56] L. Kong, Anyon condensation and tensor categories, Nucl. Phys. B **886**, 436 (2014).
[57] F. J. Burnell, Anyon condensation and its applications, Annu. Rev. Condens. Matter Phys. **9**, 307 (2018).
[58] K. Hwang, Anyon condensation and confinement transition in a Kitaev spin liquid bilayer, Physical Review B **109**, 134412 (2024).
[59] Y.-Z. You, Z. Bi, A. Rasmussen, K. Slagle, and C. Xu, Wave function and strange correlator of short-range entangled states, Phys. Rev. Lett. **112**, 247202 (2014).
[60] Y. Zou, S. Sang, and T. H. Hsieh, Channeling quantum criticality, Phys. Rev. Lett. **130**, 250403 (2023).
[61] L. Lepori, M. Burrello, A. Trombettoni, and S. Paganelli, Strange correlators for topological quantum systems from bulk-boundary correspondence, Physical Review B **108**, 035110 (2023).
[62] K. Su, N. Myerson-Jain, and C. Xu, Conformal field theories generated by Chern insulators under decoherence or measurement, Phys. Rev. B **109**, 035146 (2024).
[63] A. Sarma, Y. Bao, N. Myerson-Jain, T. Kiely, and C. Xu, Effective conformal field theory generated from pure and dephased Chern insulator, Phys. Rev. B **112**, 085130 (2025).
[64] N. Read and D. Green, Paired states of fermions in two dimensions with breaking of parity and time-reversal symmetries and the fractional quantum Hall effect, Physical Review B **61**, 10267 (2000).
[65] P. Di Francesco, P. Mathieu, and D. Sénéchal, *Conformal Field Theory* (Springer, New York, 1997).
[66] P. Ginsparg, Applied conformal field theory, in *Fields, Strings and Critical Phenomena*, Les Houches Summer School Proceedings, Vol. 49, edited by E. Brézin and J. Zinn-Justin (North-Holland, 1989) pp. 1–168, arXiv:hep-th/9108028 [hep-th].
[67] E. O'Brien and P. Fendley, Lattice supersymmetry and order-disorder coexistence in the tricritical Ising model, Physical Review Letters **120**, 206403 (2018).
[68] D. Friedan, Z. Qiu, and S. Shenker, Superconformal invariance in two dimensions and the tricritical Ising model, Phys. Lett. B **151**, 37 (1985).
[69] A. B. Zamolodchikov, From tricritical Ising to critical Ising by thermodynamic Bethe ansatz, Nuclear Physics B **358**, 524 (1991).
[70] K. J. Satzinger *et al.*, Realizing topologically ordered states on a quantum processor, Science **374**, 1237 (2021).
[71] G. Semeghini *et al.*, Probing topological spin liquids on a programmable quantum simulator, Science **374**, 1242 (2021).
[72] D. Bluvstein, H. Levine, G. Semeghini, T. T. Wang, S. Ebadi, M. Kalinowski, A. Keesling, N. Maskara, H. Pichler, M. Greiner, V. Vuletić, and M. D. Lukin, A quantum processor based on coherent transport of entangled atom arrays, Nature **604**, 451 (2022).
[73] F. L. Pedrocchi, S. Chesi, and D. Loss, Physical solutions of the kitaev honeycomb model, Phys. Rev. B **84**, 165414 (2011).
[74] E. O'Brien and P. Fendley, Lattice supersymmetry and order-

disorder coexistence in the tricritical Ising model, Phys. Rev. Lett. **120**, 206403 (2018).

Supplemental Material for "Mixed-State Topological Transition and Emergent Fractionalized Supersymmetry in the Non-Abelian Kitaev Spin Liquid"

I. VECTORIZATION CONVENTIONS AND FRACTIONALIZED HAMILTONIAN

A. Vectorization convention

At each site i, we introduce the maximally entangled state

$$|\Omega_i\rangle\!\rangle = \tfrac{1}{\sqrt{2}}\left(|\uparrow\rangle_L|\uparrow\rangle_R + |\downarrow\rangle_L|\downarrow\rangle_R\right). \tag{S12}$$

The normalized many-body reference state is $|\Omega\rangle\!\rangle = \prod_i |\Omega_i\rangle\!\rangle$. We vectorize an operator O according to

$$|O\rangle\!\rangle = (O\otimes\mathbb{1})|\Omega\rangle\!\rangle, \qquad O_L|\Omega\rangle\!\rangle = O_R^T|\Omega\rangle\!\rangle, \tag{S13}$$

where the transpose is taken in the product σ^z basis. In this convention,

$$\sigma_L^x|\Omega\rangle\!\rangle = \sigma_R^x|\Omega\rangle\!\rangle, \quad \sigma_L^y|\Omega\rangle\!\rangle = -\sigma_R^y|\Omega\rangle\!\rangle, \quad \sigma_L^z|\Omega\rangle\!\rangle = \sigma_R^z|\Omega\rangle\!\rangle. \tag{S14}$$

The bond-dephasing channel acts on the density matrix as

$$\mathcal{E}_{ij}^{\alpha}(\rho) = (1-p_\alpha)\rho + p_\alpha B_{ij}^{\alpha}\rho B_{ij}^{\alpha}, \qquad B_{ij}^{\alpha} = \sigma_i^{\alpha}\sigma_j^{\alpha}. \tag{S15}$$

Under vectorization, $|\mathcal{E}_{ij}^{\alpha}(\rho)\rangle\!\rangle = \widehat{\mathcal{E}}_{ij}^{\alpha}|\rho\rangle\!\rangle$, where the channel is represented in the doubled Hilbert space by

$$\widehat{\mathcal{E}}_{ij}^{\alpha} = (1-p_\alpha)\mathbb{1} + p_\alpha D_{ij}^{\alpha}, \qquad D_{ij}^{\alpha} = B_{ij,L}^{\alpha}B_{ij,R}^{\alpha}. \tag{S16}$$

Here we have used $(B_{ij}^{\alpha})^T = B_{ij}^{\alpha}$ in the chosen spin basis. Using $(D_{ij}^{\alpha})^2 = \mathbb{1}$, the single-bond channel can be written exactly as

$$\widehat{\mathcal{E}}_{ij}^{\alpha} = e^{-V_\alpha}e^{V_\alpha D_{ij}^{\alpha}}, \qquad e^{-2V_\alpha} = 1-2p_\alpha. \tag{S17}$$

All doubled bond operators commute: any anticommutation sign in one copy is canceled by the same sign in the other. The full channel therefore has the exact representation

$$\widehat{\mathcal{E}} = \prod_{\alpha,\langle ij\rangle_\alpha}\widehat{\mathcal{E}}_{ij}^{\alpha} \propto \exp\left(\sum_{\alpha,\langle ij\rangle_\alpha} V_\alpha D_{ij}^{\alpha}\right) \tag{S18}$$

The proportionality omits only an overall scalar; no Trotter approximation is involved.

The channel also preserves every plaquette flux. To establish this directly in the physical spin Hilbert space, label the vertices of a hexagon h cyclically by $n = 1,\ldots,6$, and let β_n denote the type of the bond leaving the plaquette at vertex n. The flux operator can be defined as

$$W_h = \prod_{n=1}^{6}\sigma_n^{\beta_n}. \tag{S19}$$

For a conventional cyclic labeling, $W_h = \sigma_1^x\sigma_2^y\sigma_3^z\sigma_4^x\sigma_5^y\sigma_6^z$. A bond not on ∂h either has disjoint support from W_h or is the outgoing bond at its only shared vertex, where the Pauli components coincide. For a bond on ∂h, the Pauli components differ at both endpoints, so the two anticommutation signs cancel. Thus, for every bond and plaquette,

$$[B_{ij}^{\alpha}, W_h] = 0. \tag{S20}$$

The channel also preserves every flux sector. In the doubled Hilbert space, the fluxes of the two copies are conserved independently:

$$[D_{ij}^{\alpha}, W_{h,L}] = [D_{ij}^{\alpha}, W_{h,R}] = 0. \tag{S21}$$

B. Majorana representation of the doubled system

We now formulate the left and right copies appearing after vectorization, together with the flux-preserving dephasing channel, in the Majorana representation. Following Ref. [32], we introduce four Majoranas at each site in each copy,

$$\sigma^{\alpha}_{i,s} = \mathrm{i}b^{\alpha}_{i,s}c_{i,s}, \qquad G_{i,s} = b^{x}_{i,s}b^{y}_{i,s}b^{z}_{i,s}c_{i,s} = +1, \qquad s = L, R. \tag{S22}$$

with the physical subspace defined by $G_{i,s} = +1$. With a slight abuse of notation, we also use $|\Omega\rangle\!\rangle$ for an unprojected reference state in the enlarged Majorana Hilbert space, chosen to satisfy

$$\begin{aligned} b^{x}_{L}|\Omega\rangle\!\rangle &= \mathrm{i}b^{x}_{R}|\Omega\rangle\!\rangle, & b^{y}_{L}|\Omega\rangle\!\rangle &= -\mathrm{i}b^{y}_{R}|\Omega\rangle\!\rangle, \\ b^{z}_{L}|\Omega\rangle\!\rangle &= \mathrm{i}b^{z}_{R}|\Omega\rangle\!\rangle, & c_{L}|\Omega\rangle\!\rangle &= -\mathrm{i}c_{R}|\Omega\rangle\!\rangle. \end{aligned} \tag{S23}$$

These phase conventions reproduce the spin-space vectorization identities in Eq. (S14) through $\sigma^{\alpha} = \mathrm{i}b^{\alpha}c$.

We introduce the $\mathbb{Z}_2$ link operator, defined on bonds by

$$u^{\alpha}_{ij,s} = -u^{\alpha}_{ji,s} = \mathrm{i}\zeta_s b^{\alpha}_{i,s}b^{\alpha}_{j,s}, \qquad \zeta_L = -\zeta_R = 1. \tag{S24}$$

The factor ζ_s compensates for the relative minus sign between the bond bilinears under Eq. (S23), so that corresponding links obey $u^{\alpha}_{ij,L}|\Omega\rangle\!\rangle = u^{\alpha}_{ij,R}|\Omega\rangle\!\rangle$. The exchange operator then becomes

$$B^{\alpha}_{ij,s} = \sigma^{\alpha}_{i,s}\sigma^{\alpha}_{j,s} = -\mathrm{i}\zeta_s u^{\alpha}_{ij,s}c_{i,s}c_{j,s}. \tag{S25}$$

Using $\zeta_L\zeta_R = -1$, the doubled bond operator becomes

$$D^{\alpha}_{ij} = u^{\alpha}_{ij,L}u^{\alpha}_{ij,R}c_{i,L}c_{j,L}c_{i,R}c_{j,R}. \tag{S26}$$

For an oriented two-bond path $i \xrightarrow{\alpha} j \xrightarrow{\beta} k$, let γ denote the remaining spin component. Using the physical constraint $G_{j,s} = 1$, the three-spin interaction can be written as

$$\sigma^{\alpha}_{i,s}\sigma^{\gamma}_{j,s}\sigma^{\beta}_{k,s} = \mathrm{i}\epsilon_{\alpha\beta\gamma}u^{\alpha}_{ij,s}u^{\beta}_{jk,s}c_{i,s}c_{k,s}, \tag{S27}$$

where $\epsilon_{\alpha\beta\gamma}$ is the Levi-Civita symbol with $\epsilon_{xyz} = +1$.

All link operators commute with one another, with each term in the Hamiltonian, and with the dephasing channel. We may therefore work in a fixed configuration $u^{\alpha}_{ij,s} = \pm 1$, subject to the zero-flux constraint

$$W_{h,s} = \prod_{\langle ij\rangle \in \partial h} u^{\alpha_{ij}}_{ij,s} = 1 \tag{S28}$$

on every hexagon, with each link in the product taken in the fixed A-to-B orientation. Throughout this work, we choose $u^{\alpha}_{ij,s} = 1$ on A-to-B bonds in the bulk of both copies. On a finite torus, the matter states must also satisfy the physical-parity constraint [73]. For the odd-L clusters used here, we impose a π boundary twist along one primitive direction. The exchange couplings change sign on bonds crossing that boundary, and each three-spin coupling acquires the product of the bond signs along its two-bond path. Taking $u^{\alpha}_{ij,s} = -1$ on these boundary-crossing bonds cancels the coupling signs, so that the matter Hamiltonians remain periodic. This choice preserves $W_h = 1$ and makes both the topological and reference vacua compatible with physical projection.

With the gauge and boundary conventions above, Eqs. (S25) and (S27) yield the periodic matter Hamiltonians

$$H_s = \zeta_s \left(\mathrm{i} \sum_{\alpha,\langle ij\rangle_\alpha} J_\alpha c_{i,s}c_{j,s} + \mathrm{i}\kappa \sum_{\langle\langle ik\rangle\rangle} \nu_{ik}c_{i,s}c_{k,s} \right), \tag{S29}$$

where $\nu_{ik} = \epsilon_{\alpha\beta\gamma} = -\nu_{ki}$ for the oriented path defined above. The right-copy spin Hamiltonian is the transpose of the left-copy Hamiltonian: the exchange terms are unchanged, whereas each three-spin term changes sign because it contains exactly one σ^y. Together with the copy-dependent link convention, this accounts for the common prefactor ζ_s. The two copies consequently have opposite matter-band Chern numbers.

Finally, define the inter-copy bilinear $\Phi_i = \mathrm{i}c_{i,L}c_{i,R}$. For isotropic dephasing, Eqs. (S26) and (S18) give

$$D^{\alpha}_{ij} = \Phi_i\Phi_j, \qquad \widehat{\mathcal{E}}(p) \propto \exp\left[V \sum_{\langle ij\rangle} \Phi_i\Phi_j \right]. \tag{S30}$$

C. Physical completion of the parton correlators

The Majoranas $c_{i,s}$ and the inter-copy bilinear Φ_i carry gauge charge. To relate their fixed-gauge correlators to physical spin observables, we connect the endpoints by gauge Wilson lines. For an oriented path γ from site i to site j, define

$$U_{\gamma,s} = \prod_{\langle lm\rangle\in\gamma} u_{lm,s}. \tag{S31}$$

Under a local gauge transformation, the signs associated with internal vertices cancel, leaving only those at the endpoints. These endpoint signs are canceled by the matter Majoranas, giving the gauge-invariant fermion string

$$\mathcal{W}_{f,s}(i,j;\gamma) = \mathrm{i}c_{i,s}U_{\gamma,s}c_{j,s}. \tag{S32}$$

Since Φ_i carries gauge charge in both copies, its two-point function requires a Wilson line in each copy:

$$\mathcal{W}_b(i,j;\gamma) = \Phi_i U_{\gamma,L}U_{\gamma,R}\Phi_j. \tag{S33}$$

These Wilson strings have a direct spin representation. For a path γ, define the spin string

$$W_{\gamma,s} \equiv \prod_{(lm)_\alpha\in\gamma} B^{\alpha}_{lm,s} = s_{\gamma,s}\mathcal{W}_{f,s}(i,j;\gamma). \tag{S34}$$

The product is ordered along γ from i to j. For a path containing ℓ_γ bonds, Eq. (S25) fixes the phase to $s_{\gamma,s} = -\mathrm{i}(-\mathrm{i}\zeta_s)^{\ell_\gamma}$. The phase product $s_{\gamma,L}s_{\gamma,R} = -1$ cancels the fermionic reordering sign in $\mathcal{W}_{f,L}\mathcal{W}_{f,R} = -\mathcal{W}_b$, giving $W_{\gamma,L}W_{\gamma,R} = \mathcal{W}_b$.

The spin strings defined above also identify the corresponding density-matrix observables. Since W_γ is real and unitary in the basis used for vectorization, $W_\gamma^T = W_\gamma^\dagger$. Its insertion a normalized Choi state therefore gives the Rényi-2 string correlator

$$C_2(W_\gamma;\rho) = \frac{\langle\!\langle\rho|W_{\gamma,L}W_{\gamma,R}|\rho\rangle\!\rangle}{\langle\!\langle\rho|\rho\rangle\!\rangle} = \frac{\mathrm{Tr}(\rho W_\gamma\rho W_\gamma^\dagger)}{\mathrm{Tr}(\rho^2)}. \tag{S35}$$

For the dephased state, we evaluate $C_2(W_\gamma;\rho_p)$ with $|\rho_p\rangle\!\rangle = \widehat{\mathcal{E}}(p)|\rho_0\rangle\!\rangle$. Since $\widehat{\mathcal{E}}(p)$ is Hermitian and the doubled Wilson string commutes with the channel, these factors can be combined. Using $D_{ij}^2 = 1$ and the mutual commutativity of the doubled bond operators, we obtain

$$\widehat{\mathcal{E}}(p)^2 = \widehat{\mathcal{E}}(q), \qquad q = 2p(1-p). \tag{S36}$$

The correlator can therefore be expressed in terms of the initial projector as

$$C_2(W_\gamma;\rho_p) = \frac{\langle\!\langle\rho_0|\widehat{\mathcal{E}}(p)W_{\gamma,L}W_{\gamma,R}\widehat{\mathcal{E}}(p)|\rho_0\rangle\!\rangle}{\langle\!\langle\rho_0|\widehat{\mathcal{E}}(p)^2|\rho_0\rangle\!\rangle} = \frac{\langle\!\langle\rho_0|W_{\gamma,L}W_{\gamma,R}\widehat{\mathcal{E}}(q)|\rho_0\rangle\!\rangle}{\langle\!\langle\rho_0|\widehat{\mathcal{E}}(q)|\rho_0\rangle\!\rangle}. \tag{S37}$$

Here p specifies the physical output state ρ_p, while q parametrizes the combined channel in this representation. Long-range order in Eq. (S37) demonstrates $\psi\bar{\psi}$ condensation in the normalized Choi state. The imTO identification does not use this correlator as a phase definition: it follows by unfolding the condensed-anyon structure at maximal dephasing, with the finite-p assignment assuming that no additional transition intervenes within the ordered branch [19, 28].

For the topological interface, the distinct topological and reference boundaries instead give the doubled-string amplitude

$$C_b^{\mathrm{str}}(i,j;\gamma) = \frac{\mathrm{Tr}\big[\rho_{\mathrm{ref}}W_\gamma\mathcal{E}_p(\rho_{\mathrm{top}})W_\gamma^\dagger\big]}{\mathrm{Tr}[\rho_{\mathrm{ref}}\mathcal{E}_p(\rho_{\mathrm{top}})]} = \frac{\langle\!\langle\rho_{\mathrm{ref}}|W_{\gamma,L}W_{\gamma,R}\widehat{\mathcal{E}}(p)|\rho_{\mathrm{top}}\rangle\!\rangle}{\langle\!\langle\rho_{\mathrm{ref}}|\widehat{\mathcal{E}}(p)|\rho_{\mathrm{top}}\rangle\!\rangle}. \tag{S38}$$

This is a type-II strange correlator because the physical string acts on both copy indices. The fermion string enters the corresponding normalized transition amplitude,

$$C_f^{\mathrm{str}}(i,j;\gamma) = \frac{\langle\!\langle\rho_{\mathrm{ref}}|W_{\gamma,L}\widehat{\mathcal{E}}(p)|\rho_{\mathrm{top}}\rangle\!\rangle}{\langle\!\langle\rho_{\mathrm{ref}}|\widehat{\mathcal{E}}(p)|\rho_{\mathrm{top}}\rangle\!\rangle}. \tag{S39}$$

This is the corresponding type-I strange correlator with a string insertion in one copy only [21]. At the supersymmetric point, $C_b^{\mathrm{str}}(r) \sim r^{-2/5}$ and $C_f^{\mathrm{str}}(r) \sim r^{-7/5}$. The equality is between their anomalous parts, not their full powers, because the fermion carries the canonical factor r^{-1}.

II. SIGN-PROBLEM-FREE QUANTUM MONTE CARLO AND SIMULATION DETAILS

A. Auxiliary-field decomposition and nonnegative weights

For isotropic dephasing, the single-bond channel admits the exact discrete Hubbard–Stratonovich representation

$$\widehat{\mathcal{E}}_{ij}(p) = e^{-V} e^{V D_{ij}^{\alpha}} = e^{-\frac{V}{2}(\mathrm{i}c_{i,L}c_{j,L}+\mathrm{i}c_{i,R}c_{j,R})^2} = \frac{1}{2}\sum_{s_{ij}=\pm 1} e^{\theta s_{ij}(c_{i,L}c_{j,L}+c_{i,R}c_{j,R})}, \quad \cos(2\theta) = e^{-2V} = 1-2p. \tag{S40}$$

Here $s_{ij} = \pm 1$ is an auxiliary Ising field on each bond. Since the interactions D_{ij}^{α} commute on different bonds, the full channel factorizes exactly into single-bond channels. Within each bond-type layer $\alpha = x, y, z$, the bonds are disjoint, so their Majorana bilinears also commute and can be grouped into a single Gaussian exponential. Applying Eq. (S40) to every bond gives

$$\widehat{\mathcal{E}}(p) = \frac{1}{2^{N_b}} \sum_{\mathcal{C}} \overrightarrow{\prod_{\alpha=x,y,z}} \exp\left[\theta \sum_{\langle ij\rangle_{\alpha}} s_{ij}\left(c_{i,L}c_{j,L} + c_{i,R}c_{j,R}\right)\right], \tag{S41}$$

where N_b is the total number of bonds, $\mathcal{C} = \{s_{ij}\}$ denotes an auxiliary-field configuration, and the arrow specifies a fixed ordering of the three bond layers. For a fixed $\mathcal{C}$, Gaussian factors in different layers generally do not commute, so this ordering is retained explicitly. The auxiliary-field sum nevertheless reproduces the channel exactly, with no Trotter approximation.

Let $\mathcal{G}_s(\mathcal{C})$ denote the ordered product of Gaussian factors acting on copy s in Eq. (S41). We consider boundary states $|\rho_a\rangle\!\rangle$, $|\rho_b\rangle\!\rangle$, with complex-conjugate partners in the two copies, $|\psi_{a,R}\rangle = |\psi_{a,L}^*\rangle$ and similarly for b. The channel overlap between these doubled boundary states is $Z_{ab} = \sum_{\mathcal{C}} w_{ab}(\mathcal{C})$, where

$$w_{ab}(\mathcal{C}) = \frac{1}{2^{N_b}} \prod_{s=L,R} \langle\psi_{a,s}|\mathcal{G}_s(\mathcal{C})|\psi_{b,s}\rangle. \tag{S42}$$

For a fixed auxiliary-field configuration, the Hubbard–Stratonovich factors preserve the conjugate relation between the two copies. Consequently, $\langle\psi_{a,R}|\mathcal{G}_R(\mathcal{C})|\psi_{b,R}\rangle = [\langle\psi_{a,L}|\mathcal{G}_L(\mathcal{C})|\psi_{b,L}\rangle]^*$, and hence

$$w_{ab}(\mathcal{C}) = \frac{1}{2^{N_b}} \left|\langle\psi_{a,L}|\mathcal{G}_L(\mathcal{C})|\psi_{b,L}\rangle\right|^2 \geq 0. \tag{S43}$$

This conjugate pairing eliminates the fermion sign problem configuration by configuration [51–53]. Configurations are sampled with probability $w_{ab}(\mathcal{C})/Z_{ab}$.

B. Gaussian overlaps and correlation estimators

To evaluate the single-copy overlap $A_{ab}(\mathcal{C}) = \langle\psi_{a,L}|\mathcal{G}_L(\mathcal{C})|\psi_{b,L}\rangle$, we write

$$\mathcal{G}_L(\mathcal{C}) = \overrightarrow{\prod_{\alpha=x,y,z}} \exp\left[\frac{1}{4}\boldsymbol{c}_L^T K_{\alpha}(\mathcal{C})\boldsymbol{c}_L\right]. \tag{S44}$$

Here K_{α} is an antisymmetric matrix with $(K_{\alpha})_{ij} = -(K_{\alpha})_{ji} = 2\theta s_{ij}$ on each α bond directed from A to B, and all other entries zero. Following Ref. [51], we introduce an identical auxiliary Majorana copy $\widetilde{c}_{i,L}$, distinct from the vectorization copy R, and define $f_i = (c_{i,L} + \mathrm{i}\widetilde{c}_{i,L})/2$. The two identical Gaussian generators then combine into a number-conserving form,

$$\frac{1}{4}\boldsymbol{c}_L^T K_{\alpha}\boldsymbol{c}_L + \frac{1}{4}\widetilde{\boldsymbol{c}}^T K_{\alpha}\widetilde{\boldsymbol{c}} = \boldsymbol{f}^{\dagger} K_{\alpha}\boldsymbol{f}. \tag{S45}$$

Likewise, pairing each boundary state with its identical auxiliary copy gives a Slater determinant $|F_a\rangle = |\psi_{a,L}\rangle \otimes |\widetilde{\psi}_{a,L}\rangle$. Let P_a denote its $N \times (N/2)$ occupied-orbital matrix, and similarly for P_b. For ground-state boundaries, these orbitals are obtained by diagonalizing the corresponding duplicated boundary Hamiltonian. The squared overlap becomes

$$A_{ab}(\mathcal{C})^2 = \langle F_a| \overrightarrow{\prod_{\alpha=x,y,z}} e^{\boldsymbol{f}^{\dagger} K_{\alpha}(\mathcal{C})\boldsymbol{f}} |F_b\rangle = \det M_{ab}(\mathcal{C}), \quad M_{ab}(\mathcal{C}) = P_a^{\dagger}\left[\overrightarrow{\prod_{\alpha=x,y,z}} e^{K_{\alpha}(\mathcal{C})}\right] P_b. \tag{S46}$$

Using $|A_{ab}|^2 = |A_{ab}^2|$, the nonnegative sampling weight therefore takes the determinant form

$$w_{ab}(\mathcal{C}) = \frac{1}{2^{N_b}} \left|\det M_{ab}(\mathcal{C})\right|. \tag{S47}$$

The determinant representation allows standard determinant quantum Monte Carlo techniques to be used for matrix updates and Green-function evaluation. For each auxiliary-field configuration, we define the normalized transition Green function

$$g_{ij,s}(\mathcal{C}) = \frac{\langle\psi_{a,s}|c_{i,s}c_{j,s}\mathcal{G}_s(\mathcal{C})|\psi_{b,s}\rangle}{\langle\psi_{a,s}|\mathcal{G}_s(\mathcal{C})|\psi_{b,s}\rangle}. \tag{S48}$$

Using the Slater-determinant representation, the transition Green function is

$$g_{ij,L}(\mathcal{C}) = 2\left[\left(\prod_{\alpha=x,y,z}^{\rightarrow} e^{K_\alpha(\mathcal{C})}\right) P_b M_{ab}(\mathcal{C})^{-1} P_a^\dagger\right]_{ji}, \qquad g_{ij,R}(\mathcal{C}) = g_{ij,L}(\mathcal{C})^*. \tag{S49}$$

The factor of two follows from $\langle f_i^\dagger f_j\rangle_{\mathcal{C}} = g_{ij,L}(\mathcal{C})/2$ in the identical auxiliary-copy construction.

Since the two copies decouple at fixed $\mathcal{C}$, the bosonic and fermionic correlators are obtained as

$$\begin{aligned}\langle\Phi_i\Phi_j\rangle_{ab} &= \langle g_{ij,L}(\mathcal{C})g_{ij,R}(\mathcal{C})\rangle_{\mathrm{MC}} = \left\langle|g_{ij,L}(\mathcal{C})|^2\right\rangle_{\mathrm{MC}},\\ \langle c_{i,L}c_{j,L}\rangle_{ab} &= \langle g_{ij,L}(\mathcal{C})\rangle_{\mathrm{MC}}.\end{aligned} \tag{S50}$$

Here $\langle\cdots\rangle_{\mathrm{MC}}$ denotes averaging with probability $w_{ab}(\mathcal{C})/Z_{ab}$. Higher-order correlation functions are evaluated using Wick's theorem at fixed $\mathcal{C}$ before Monte Carlo averaging. For the normalized output Choi state, the same bosonic estimator applies with identical initial boundary states and effective channel probability $q = 2p(1-p)$ as shown in Eq. (S37).

C. Observables and finite size scaling

In the simulation, we use periodic honeycomb clusters with $L \times L$ unit cells, $N = 2L^2$ sites. The primitive and reciprocal vectors are

$$\mathbf{a}_{1,2} = \left(\frac{1}{2}, \pm\frac{\sqrt{3}}{2}\right), \qquad \mathbf{b}_{1,2} = 2\pi\left(1, \pm\frac{1}{\sqrt{3}}\right), \tag{S51}$$

with $\mathbf{a}_\mu \cdot \mathbf{b}_\nu = 2\pi\delta_{\mu\nu}$. We label sites by a unit-cell coordinate $\mathbf{R} = n_1\mathbf{a}_1 + n_2\mathbf{a}_2$ and a sublattice index $\mu = A, B$. Allowed momenta are $\mathbf{q} = (m_1\mathbf{b}_1 + m_2\mathbf{b}_2)/L$, and we choose $\mathbf{q}_{\min} = \mathbf{b}_1/L$.

Using the bosonic correlators defined above, the same-sublattice structure factor is

$$S_{\Phi,\mu\mu}(\mathbf{q}) = \frac{1}{L^2}\sum_{\mathbf{R},\mathbf{R}'} e^{\mathrm{i}\mathbf{q}\cdot(\mathbf{R}-\mathbf{R}')}\langle\Phi_{\mathbf{R},\mu}\Phi_{\mathbf{R}',\mu}\rangle. \tag{S52}$$

The squared order parameter and dimensionless correlation ratio are

$$m^2_{\Phi,\mu\mu} = \frac{S_{\Phi,\mu\mu}(\mathbf{0})}{L^2}, \qquad R_{\Phi,\mu\mu} = 1 - \frac{S_{\Phi,\mu\mu}(\mathbf{q}_{\min})}{S_{\Phi,\mu\mu}(\mathbf{0})}. \tag{S53}$$

These definitions apply to both the normalized-output and temporal-interface calculations, using their respective correlators.

For the temporal interface, we additionally measure the window-averaged fermionic correlation

$$\overline{\mathcal{C}}^{\mathrm{win}}_{f,\mu\mu} = \frac{1}{|\mathcal{W}_L|}\sum_{\mathbf{d}\in\mathcal{W}_L}\left|\frac{1}{L^2}\sum_{\mathbf{R}}\langle c_{\mathbf{R},\mu,L}c_{\mathbf{R}+\mathbf{d},\mu,L}\rangle_{\mathrm{str}}\right|. \tag{S54}$$

The window $\mathcal{W}_L$ contains displacements $\mathbf{d} = d_1\mathbf{a}_1 + d_2\mathbf{a}_2$ with integer $L/3 \le d_1, d_2 \le 2L/3$. The absolute value is taken after averaging the correlator, and the window selects separations proportional to L.

All simulations are performed at $J_x = J_y = 1$ and $\kappa = 0.5$, with isotropic dephasing. We discard the first 500 sweeps of each independent Markov chain for equilibration. Each sweep updates all bonds in the fixed x, y, z layer order, followed by

measurements. Green functions are restabilized every five sweeps. We analyze the critical behavior using the finite-size scaling forms

$$\begin{aligned} R_\Phi &= F_R(x) + L^{-\omega} G_R(x), \\ m_\Phi^2 &= L^{-\eta_b} \left[F_b(x) + L^{-\omega} G_b(x) \right], \\ \overline{\mathcal{C}}_f^{\mathrm{win}} &= L^{-1-\eta_f} \left[F_f(x) + L^{-\omega} G_f(x) \right]. \end{aligned} \tag{S55}$$

Here $x = (p - p_c)L^{1/\nu}$, and the AA sublattice subscripts are omitted. Other sublattice channels exhibit consistent critical behavior. The scaling functions F_a and correction functions G_a are approximated by polynomials of degree m and n, respectively. The correction exponent ω is specified separately for each observable below.

For the Choi-state calculation, we take $J_z = 1$ for both boundary states. The bosonic string operators commute with the channel, allowing the two channel factors in the correlator to combine as $\widehat{\mathcal{E}}(p)^2 = \widehat{\mathcal{E}}(q)$, where $q = 2p(1-p)$ and p is the physical dephasing probability. We fit the data for $21 \le L \le 51$ and $|p - 0.167| \le 0.009$, using $m = 7$ and $n = 2$. The correlation-ratio correction exponent is poorly constrained, so we fix $\omega = 2$ to stabilize the fit; the bosonic correction exponent is fitted independently. The correlation-ratio fit gives $p_c^{(2)} = 0.16687(8)$ and $\nu = 1.011(16)$, with $\chi^2/\mathrm{dof} = 0.655$. Fixing these two parameters in the subsequent fit of m_Φ^2 yields $\eta = 0.246(11)$, with $\chi^2/\mathrm{dof} = 1.031$. These estimates are consistent with the two-dimensional Ising exponents $\nu = 1$ and $\eta = 1/4$.

For the topological-interface calculation, we choose $J_z = 3$ and $J_z = 1$ for the bra and ket boundary states, respectively. The data in Fig. 3(a)–(c) are obtained from $(3.20\text{–}3.36) \times 10^5$ Monte Carlo sweeps per point. We supplement these data with independent simulations at $p = 0.23, 0.2451513, 0.25$ and $L = 21, 27, \ldots, 57$, using 32–384 Markov chains and a total of $(1.68\text{–}1.73) \times 10^6$ sweeps per point. All sweep counts refer to sampling after equilibration and are summed over chains. We fit the combined data for $21 \le L \le 57$ and $|p - 0.2452| \le 0.012$, using $m = 6$ and $n = 2$. As in the Choi-state analysis, we fix $\omega = 2$ for the correlation ratio and allow the bosonic and fermionic correction exponents to vary independently. The resulting estimates are $p_c = 0.24526(6)$, $\nu = 1.27(3)$, $\eta_b = 0.405(6)$, and $\eta_f = 0.395(21)$. The corresponding χ^2/dof values are $57.56/50$, $55.57/50$, and $62.77/50$ for the correlation-ratio, bosonic, and fermionic fits, respectively.

To compare the spatial anisotropies of the two sectors, we evaluate the translation-averaged AA correlators $C_a(\mathbf{d})$, with $a = b, f$, at $\mathbf{d}_\pm = \frac{L}{3}(\mathbf{a}_1 \pm \mathbf{a}_2)$. For the lattice convention used here, $\mathbf{d}_+ = (L/3, 0)$ and $\mathbf{d}_- = (0, \sqrt{3}L/3)$. Motivated by the anisotropic power-law form $|C_a(x,y)| \propto [x^2 + (y/\lambda_a)^2]^{-\alpha_a/2}$, we define

$$\lambda_a^{\mathrm{eff}}(L) = \sqrt{3} \left| \frac{C_a(\mathbf{d}_-)}{C_a(\mathbf{d}_+)} \right|^{1/\alpha_a}, \qquad \alpha_b = \frac{2}{5}, \quad \alpha_f = \frac{7}{5}. \tag{S56}$$

The powers are fixed to the supersymmetric predictions. Since the separations remain fixed fractions of L, λ_a^{eff} provides a finite-size measure of correlation anisotropy. We use the high-statistics data at $p = 0.23, p_*, 0.25$, where $p_* = 0.2451513$ denotes the near-critical simulation point. The relative anisotropy is quantified by

$$\Delta_\lambda(L) = \log \frac{\lambda_f^{\mathrm{eff}}(L)}{\lambda_b^{\mathrm{eff}}(L)}, \qquad \Delta_\lambda(L) = \Delta_\lambda^{(\infty)} + \frac{A_\lambda}{L}. \tag{S57}$$

At each probability, we fit the data for $L = 33, 39, \ldots, 57$ with a free intercept. Error bars are obtained from a paired delete-one-chain jackknife applied to the full estimator. For the near-critical dataset, the extrapolation gives $\Delta_\lambda^{(\infty)} = 0.006(19)$, consistent with vanishing boson–fermion anisotropy mismatch.

III. FROM DOUBLED-ISING ORDER TO INTRINSIC MIXED-STATE TOPOLOGICAL ORDER

A. Condensation in the normalized Choi state

The chiral non-Abelian phase of one Kitaev copy has Ising anyons $\{1, \sigma, \psi\}$, quantum dimensions $d_1 = d_\psi = 1$, $d_\sigma = \sqrt{2}$, and fusion rules

$$\psi \times \psi = 1, \qquad \psi \times \sigma = \sigma, \qquad \sigma \times \sigma = 1 + \psi. \tag{S58}$$

Their topological spins are $\theta_1 = 1$, $\theta_\psi = -1$, and $\theta_\sigma = e^{\mathrm{i}\pi/8}$ [32, 33]. Vectorizing a pure density matrix produces the nonchiral product $\mathrm{Ising} \boxtimes \overline{\mathrm{Ising}}$, whose nine sectors are denoted $a\bar{b}$.

The channel interaction creates the inter-copy pair $b_c = \psi\bar{\psi}$. It is an Abelian boson because $d_{b_c} = 1$ and $\theta_{b_c} = \theta_\psi \theta_{\bar{\psi}} = 1$. An anyon remains deconfined after condensation only if its monodromy with b_c is trivial. The five sectors satisfying this condition are

$$1\bar{1}, \quad \psi\bar{\psi}, \quad \psi\bar{1}, \quad 1\bar{\psi}, \quad \sigma\bar{\sigma}. \tag{S59}$$

The other four sectors with exactly one σ have nontrivial monodromy and are confined.

Fusion with the condensate produces the identifications

$$1\bar{1} \sim \psi\bar{\psi} \equiv 1, \qquad \psi\bar{1} \sim 1\bar{\psi} \equiv \epsilon. \tag{S60}$$

The sector $\sigma\bar{\sigma}$ is a fixed point under fusion with b_c and has quantum dimension two, so it must split into two Abelian sectors,

$$\sigma\bar{\sigma} \longrightarrow e + m. \tag{S61}$$

This splitting is also required by its fusion square:

$$(\sigma\bar{\sigma})^2 = (1+\psi)(\bar{1}+\bar{\psi}) = 1\bar{1} + \psi\bar{\psi} + \psi\bar{1} + 1\bar{\psi} \longrightarrow 2(1+\epsilon), \tag{S62}$$

which equals $(e+m)^2$ for toric-code fusion. The descendants obey $e^2 = m^2 = \epsilon^2 = 1$ and $e \times m = \epsilon$, with $\theta_e = \theta_m = 1$ and $\theta_\epsilon = -1$. The total quantum dimension changes from $\mathcal{D}_{\mathrm{Ising}\boxtimes\overline{\mathrm{Ising}}} = 4$ to $\mathcal{D}_{\mathrm{TC}} = 2$, as expected after condensation of an algebra of dimension two [28, 55–57].

B. Unfolding to the density matrix

The doubled-state result cannot be interpreted literally as a physical bilayer. Under the inverse Choi map,

$$a\bar{b}|\rho\rangle\!\rangle \quad \longleftrightarrow \quad W_a \rho W_b^\dagger, \tag{S63}$$

where W_a and W_b are string operators carrying the corresponding topological charges. At the maximal-dephasing fixed point, doubled condensation $\psi\bar{\psi}$ makes the mixed state invariant under inserting a closed ψ string on the ket and bra simultaneously. This operation gauges out ψ in operator space rather than erasing the distinction between a one-sided ψ and the vacuum [28].

After unfolding, the deconfined one-sided content is generated by $\{1, \psi\}$. Because ψ braids trivially with every surviving sector while retaining fermionic spin, it lies in the transparent center of the braided category. The category is therefore nonmodular, which is forbidden for the complete anyon theory of a strictly two-dimensional bosonic gapped ground state but is consistent for a mixed density matrix [28]. This fixed point is consequently intrinsically mixed-state topological order. We identify the finite-p ordered branch with the same imTO phase provided it is connected to the fixed point without an intervening transition.

This construction can be stated precisely as higher-form SW-SSB. For a closed Wilson loop $W_a(\Gamma)$, strong invariance means that its left and right actions stabilize the density matrix separately, whereas weak invariance requires only the diagonal action $W_a(\Gamma)\rho W_a^\dagger(\Gamma) = \rho$. Incoherently proliferating short ψ strings preserves a one-sided loop only when its monodromy with ψ is trivial. Since $M_{\psi,\psi} = +1$, the ψ Wilson-loop symmetry remains strong. Here $M_{a,b}$ denotes the monodromy between anyon a and b. By contrast, $M_{\sigma,\psi} = -1$: a one-sided σ loop detects the proliferated ψ strings and is no longer a strong symmetry, but the signs cancel for its simultaneous ket–bra action. The non-invertible one-form symmetry generated by the σ line is therefore reduced from strong to weak, while the surviving strong sector is $\{1, \psi\}$. Because the surviving fermion is transparent, that sector is nonmodular, giving the one-form-symmetry characterization of the imTO fixed point [8, 28, 29].

IV. GAPLESS MAJORANA AT THE TEMPORAL INTERFACE

A. Bloch Hamiltonian and Chern phases

We set $J_x = J_y = J > 0$ and use primitive vectors $\boldsymbol{a}_1 = (1/2, \sqrt{3}/2)$ and $\boldsymbol{a}_2 = (1/2, -\sqrt{3}/2)$. With $k_a = \boldsymbol{k} \cdot \boldsymbol{a}_a$, the uniform-gauge Majorana Hamiltonian has the two-sublattice form for the left copy (the right copy is the complex conjugate)

$$h(\boldsymbol{k}) = d_x(\boldsymbol{k})\tau^x + d_y(\boldsymbol{k})\tau^y + d_z(\boldsymbol{k})\tau^z, \tag{S64}$$

where τ acts on sublattices and

$$d_x - \mathrm{i}d_y = \mathrm{i}\left(J_z + Je^{-\mathrm{i}k_1} + Je^{\mathrm{i}k_2}\right), \qquad d_z = \kappa\left[-\sin k_1 - \sin k_2 + \sin(k_1 + k_2)\right]. \tag{S65}$$

We can analyze the gap closing point and deduce the Chern number. At $\Gamma = (0,0)$ and $M_1 = (\pi,0)$, $M_2 = (0,\pi)$, $M_3 = (\pi,-\pi)$, the time-reversal-breaking term vanishes. The four real masses are

$$m_\Gamma = J_z + 2J, \qquad m_1 = m_2 = J_z, \qquad m_3 = J_z - 2J. \tag{S66}$$

Their signs determine the Chern number of the occupied matter-Majorana band, as summarized in Table S1.

Supplemental Table S1. Mass signs and Chern number for $J_x = J_y = J > 0$ and $\kappa > 0$.

range of J_z	$(m_\Gamma, m_1, m_2, m_3)$	C
$J_z < -2J$	$(-,-,-,-)$	0
$-2J < J_z < 0$	$(+,-,-,-)$	-1
$0 < J_z < 2J$	$(+,+,+,-)$	$+1$
$J_z > 2J$	$(+,+,+,+)$	0

The gap closes at Γ when $J_z = -2J$, at M_1 and M_2 when $J_z = 0$, and at M_3 when $J_z = 2J$. In particular, the selected strange-correlator geometry uses

$$0 < J_z^{\rm top} < 2J, \qquad J_z^{\rm ref} > 2J, \tag{S67}$$

so only m_3 changes sign. The topological mismatch is $\Delta C = 1$ and the temporal interface carries one Majorana mode at M_3.

For completeness, the other possible trivial references expose different sets of modes:

$$\begin{aligned} -2J < J_z^{\rm top} < 0,\ J_z^{\rm ref} < -2J: &\quad \Gamma, \\ -2J < J_z^{\rm top} < 0,\ J_z^{\rm ref} > 2J: &\quad M_1, M_2, M_3, \\ 0 < J_z^{\rm top} < 2J,\ J_z^{\rm ref} < -2J: &\quad \Gamma, M_1, M_2. \end{aligned} \tag{S68}$$

The single-M_3 choice avoids additional flavors and the anisotropic multicritical mode at Γ.

B. Long-wavelength modes

Expanding Eq. (S64) about the M_3 point gives,

$$h_{M_3}(\boldsymbol{q}) = -\sqrt{3}Jq_y\tau^x + 2\kappa q_x\tau^z - m_3\tau^y. \tag{S69}$$

with velocities $v_x = 2\kappa$ and $v_y = \sqrt{3}J$. We now derive the temporal-interface correlator and the quadratic action quoted in the main text. Combine the two matter Majoranas into $f_{\boldsymbol{q}} = (c_{A,\boldsymbol{q}} + \mathrm{i}c_{B,-\boldsymbol{q}})/2$ and use the Nambu spinor $\Psi_{\boldsymbol{q}} = (f_{\boldsymbol{q}}, f^\dagger_{-\boldsymbol{q}})^T$. The singular M_3 block can be written as

$$h_{\rm BdG}(\boldsymbol{q}) = \begin{pmatrix} \varepsilon_{\boldsymbol{q}} & \Delta_{\boldsymbol{q}} \\ \Delta^*_{\boldsymbol{q}} & -\varepsilon_{\boldsymbol{q}} \end{pmatrix}, \qquad \varepsilon_{\boldsymbol{q}} = m_3 + O(q^2), \qquad \Delta_{\boldsymbol{q}} = v_x q_x - \mathrm{i}v_y q_y + O(q^2), \tag{S70}$$

The negative-energy eigenmode gives the BCS form

$$|\Psi\rangle = \mathcal{N}^{-1}\prod_{\boldsymbol{q}>0}\left(1 - g_{\boldsymbol{q}} f^\dagger_{\boldsymbol{q}} f^\dagger_{-\boldsymbol{q}}\right)|0\rangle, \qquad g_{\boldsymbol{q}} = \frac{\xi_{\boldsymbol{q}} - \varepsilon_{\boldsymbol{q}}}{\Delta^*_{\boldsymbol{q}}}, \qquad \xi_{\boldsymbol{q}} = (\varepsilon^2_{\boldsymbol{q}} + |\Delta_{\boldsymbol{q}}|^2)^{1/2} \tag{S71}$$

In the topological state $m_3 < 0$, the numerator approaches a nonzero constant as $\boldsymbol{q} \to 0$; the trivial state with $m_3 > 0$ may be adiabatically flattened to the vacuum without changing the singular part of the transition amplitude. Therefore, a straightforward calculation yields,

$$\begin{aligned} \frac{\langle \Psi_{\rm ref}| f_{\boldsymbol{q},L} f_{-\boldsymbol{q},L}|\Psi_{\rm top}\rangle}{\langle \Psi_{\rm ref}|\Psi_{\rm top}\rangle} &\sim \frac{1}{v_x q_x + \mathrm{i}v_y q_y}, \\ \frac{\langle \Psi^*_{\rm ref}| f_{\boldsymbol{q},R} f_{-\boldsymbol{q},R}|\Psi^*_{\rm top}\rangle}{\langle \Psi^*_{\rm ref}|\Psi^*_{\rm top}\rangle} &\sim \frac{1}{-v_x q_x + \mathrm{i}v_y q_y}. \end{aligned} \tag{S72}$$

where in the second line, we use the time-reversal conjugate to get the right copy.

These are precisely the diagonal propagators of the two-component real field $\chi = (\chi_L, \chi_R)^T$ with action

$$S_M[\chi] = \frac{1}{2}\int \frac{d^2q}{(2\pi)^2}\, \chi^T(-\boldsymbol{q})\,(\mathrm{i}v_y q_y \mathbb{1} + v_x q_x \sigma^z)\,\chi(\boldsymbol{q}). \tag{S73}$$

Here σ^z acts on the copy/chirality index, whereas $\tau^{x,y,z}$ in Eq. (S64) acts on the microscopic sublattice spinor. χ_L and χ_R are the two chiral components exchanged by the time-reversal-like copy symmetry; together they constitute one nonchiral Majorana field, namely the $c = 1/2$ Ising CFT.

V. TRICRITICAL-ISING ENDPOINT AND SUPERSYMMETRIC EXPONENTS

The most general local continuum action needed near the single-M_3 interface is

$$S[\chi,\phi] = S_M[\chi] + \int d^2x \left[\frac{1}{2}(\partial\phi)^2 + \frac{r}{2}\phi^2 + \frac{u}{4!}\phi^4 + g\phi\,\mathrm{i}\chi_R\chi_L\right]. \tag{S74}$$

Here ϕ is a real scalar corresponding to the inter-copy fermion bilinear. Through the Jordan–Wigner equivalence, the massless Majorana theory is the critical Ising model, which admits a bosonic description in terms of the order-parameter field σ. The Majorana bilinear $i\chi_R\chi_L$ is the fermion mass operator and maps to the Ising thermal operator ϵ, represented by σ^2 in Landau–Ginzburg theory:

$$\mathrm{i}\chi_R\chi_L \sim \epsilon \sim \sigma^2. \tag{S75}$$

A Landau–Ginzburg representation that keeps both fields is therefore

$$S[\sigma,\phi] = \int d^2x \left[\frac{1}{2}(\partial\sigma)^2 + \frac{r_\sigma}{2}\sigma^2 + \frac{u_\sigma}{4}\sigma^4 + \frac{w_\sigma}{6}\sigma^6 + g\phi\sigma^2 + \frac{1}{2}(\partial\phi)^2 + \frac{r}{2}\phi^2 + \frac{u}{4!}\phi^4\right]. \tag{S76}$$

The Chern-number mismatch supplies one chiral interface branch in each copy. The mass $\mathrm{i}\chi_R\chi_L$ is nevertheless forbidden in the symmetric phase by the independent copy parities $\mathbb{Z}^f_{2,L} \times \mathbb{Z}^f_{2,R}$. Because changing p preserves these parities, the dephasing trajectory obeys

$$r_\sigma = 0 \tag{S77}$$

until the inter-copy field condenses and breaks them to diagonal parity. Integrating out the bare-massive component of ϕ gives, to leading order,

$$S_{\text{eff}} = \int d^2x \left[\frac{1}{2}(\partial\sigma)^2 + \frac{u_\sigma^{\text{eff}}}{4}\sigma^4 + \frac{w_\sigma}{6}\sigma^6\right], \qquad u_\sigma^{\text{eff}} = u_\sigma - \frac{2g^2}{r}\,. \tag{S78}$$

Thus dephasing tunes the interaction within the massless manifold. The three regimes are

$$\begin{aligned} &u_\sigma^{\text{eff}} > 0 \;:\; \text{Majorana/Ising critical phase}, \quad c = 1/2,\\ &u_\sigma^{\text{eff}} = 0 \;:\; \text{tricritical-Ising endpoint}, \quad c = 7/10,\\ &u_\sigma^{\text{eff}} < 0 \;:\; \text{massive phase}. \end{aligned} \tag{S79}$$

The tricritical-Ising CFT is the $\mathcal{N} = 1$ supersymmetric minimal model with central charge $c = 7/10$. The multiplet relevant here contains the bosonic primary ϵ, its fermionic descendant ψ_ϵ, and the bosonic superdescendant ϵ':

$$x_\epsilon = \frac{1}{5}, \qquad x_{\psi_\epsilon} = \frac{7}{10}, \qquad x_{\epsilon'} = \frac{6}{5}. \tag{S80}$$

Their dimensions differ successively by $1/2$, as required by the supercharges [44, 68, 74]. The microscopic inter-copy boson overlaps with ϵ, while the interface Majorana overlaps with ψ_ϵ. In two Euclidean dimensions this gives

$$\langle\phi(r)\phi(0)\rangle \sim r^{-2x_\epsilon} = r^{-2/5}, \qquad \langle\chi(r)\chi(0)\rangle \sim r^{-2x_{\psi_\epsilon}} = r^{-7/5}. \tag{S81}$$

With the conventional definitions $\langle\phi(r)\phi(0)\rangle \sim r^{-\eta_b}$ and $\langle\chi(r)\chi(0)\rangle \sim r^{-(1+\eta_f)}$, Eq. (S81) yields $\eta_b = \eta_f = \frac{2}{5}$.

Changing the dephasing probability preserves Eq. (S77) and therefore couples to ϵ', not to ϵ. Its renormalization-group eigenvalue and correlation-length exponent are

$$y_p = 2 - x_{\epsilon'} = \frac{4}{5}, \qquad \nu_p = \frac{1}{y_p} = \frac{5}{4}. \tag{S82}$$

A generic perturbation perpendicular to the topological interface trajectory directly changes the Majorana mass and couples to ϵ instead:

$$y_\perp = 2 - x_\epsilon = \frac{9}{5}, \qquad \nu_\perp = \frac{5}{9}. \tag{S83}$$

The distinction between Eqs. (S82) and (S83) is essential: $5/4$ is a property of the topology-constrained dephasing path, not the generic thermal exponent of tricritical Ising.